Intersection Signal-Vehicle Coupled Coordination with Mixed Autonomy Vehicles

Mingyang Chen, Bingbing Li, Yougang Bian, Weichao Zhuang, Simos A Evangelou, Xiao Pan and Boli Chen

***Abstract*—Connected and autonomous vehicles (CAVs) are predicted to alleviate traffic congestion, particularly at road intersections, which are the major bottleneck of the urban road network. This paper proposes a signal-vehicle coupled optimal control strategy for mixed traffic flows of CAVs and human-driven vehicles. The method follows a two-layer architecture, which formulates the signal-vehicle control tasks as two cascaded optimization problems by a notion of mixed platoons so that they can be efficiently solved by the central coordinator. In particular, the upper layer is designed to minimize the total waiting time of all vehicles in the intersection, while the lower layer is formulated to minimize the aggregated vehicle energy consumption by adequately exploiting the signal plan, number of crossing vehicles and target crossing speed obtained in the upper layer. Extensive simulation results are provided to examine the performance of the proposed signal-vehicle joint control framework and to reveal the impact of the introduction of the new algorithm at different CAV penetration rates, traffic demands and electric vehicle ratios. The comparisons with existing methods demonstrate the benefit of the proposed method in terms of fuel usage and traffic throughput.**

NOMENCLATURE

$a^q_{l,i,j}$	Vehicle acceleration
$D^q_{l,j}$, $\lambda^q_{l,i,j}$	Lengths of a platoon and a vehicle
$\mathcal{J}$, $\mathcal{V}$, $\mathcal{P}$	Sets of road lanes, vehicles and platoons
$\mathcal{L}(\bar{\mathcal{L}})$	Set of platoon orders (queue included)
l^{q*}_j	Optimal number of platoons to cross in qth phase and jth lane
L_{ComZ}, L_{CZ}, L_{MZ}	Lengths of communication, control and merging zones
$p^q_{l,i,j}$	Vehicle position
$\mathcal{S}^q$	Information set of the qth signal phase
$s^q_{l,i,j}$	Vehicle headway distance
s_0	Standstill spacing between vehicles
$T_{n^q_j}$	Discharging time required for the queue in qth phase and jth lane
T_0	Safe time headway
T^q, T^{q*}	SPAT duration of qth signal phase and its optimal value
t	Independent time variable
t^q	Start time of the qth signal phase
$\tilde{t}_{l,j}$, $\bar{t}_{l,j}$	Platoon ComZ and CZ entering time
$t^{wait}_{l,j}$	Platoon waiting time at the intersection
$t^q_{f,l,j}$	Target crossing time of lth platoon in the jth lane
$u^q_{l,j}(t)$, $\tau^q_{l,j}(t)$	CAV control input and time-lag
$v^q_{l,i,j}$	Vehicle velocity
v^{q*}_j, s^{q*}_j	Target driving speed and headway distance in the CZ
$\Phi^q_{l,i,j}$, $\phi^q_{l,i,j}$	Vehicle fuel consumption and its rate of change

Subscripts and superscripts

i, j, l, q	Index of vehicles, intersection road lanes, platoons and signal phase
$\hat{}$	Estimate
*	Optimum or steady state

I. INTRODUCTION

The advent of connected and autonomous vehicles (CAVs) that feature advanced sensing, communication, and control capability, presents a potential solution to these issues by offering a more responsive, cooperative, and efficient mode of transportation compared to traditional vehicles, thereby addressing the aforementioned concerns and promoting a more fluid flow of traffic [1], [2]. Most of the research on cooperative vehicle control is proposed for highway scenarios, referred to as unidimensional platooning. When it comes to urban scenarios, intersections represent the main bottlenecks that require 2D vehicle cooperation. In particular, vehicle trajectories are optimized subject to priority rules at the intersection so that they can safely and efficiently cross the intersection. Despite the rich literature on intersection management, most of the existing work considers a fully autonomous scenario [3]–[8]. However, there exists a transition period for road vehicles from current human-driven vehicles (HDV) to CAVs [9]. To address the complex behavior of HDVs, a large amount of research has been dedicated to developing safety assurance methods, with a particular focus on learning-based control strategies [10]. Recently, an unsignalized intersection coordination method using reinforcement learning was developed in [7]. This method employs conditional value-at-risk to create uncertainty-aware driving profiles for CAVs. Such a strategy shows promise for application in scenarios with mixed traffic. Moreover, traffic signals are expected to continue playing a crucial role in the safe coordination of traffic involving both CAV and HDV at road intersections. Traffic signals and vehicles are traditionally studied separately for signalized intersections [11]–[15]. However, the signal and vehicle velocity are mutually coupled.

This work has been supported by The Royal Society Grant, IES\R2\212041. (*Corresponding author: Boli Chen*)

M. Chen and B. Chen are with the Dept. of Electronic and Electrical Engineering, University College London, UK (e-mail: mingyang.chen.21@ucl.ac.uk; boli.chen@ucl.ac.uk).

W. Zhuang and B. Li are with the School of Mechanical Engineering, Southeast University, Nanjing, 211189, China (e-mail: wezhuang@seu.edu.cn; bingbli@seu.edu.cn).

X. Pan and S. A. Evangelou are with the Dept. of Electrical and Electronic Engineering at Imperial College London, UK (e-mail: xiao.pan17@imperial.ac.uk; s.evangelou@imperial.ac.uk).

Y. Bian is with State Key Lab of Advanced Design and Manufacturing for Vehicle Body, College of Mechanical and Vehicle Engineering, Hunan University, Changsha, China

Individual traffic signal or vehicle control is not sufficient to ensure traffic efficiency at a road intersection.

A common solution to address signal and vehicle-coupled coordination problems is a two-layered structure for SPAT and vehicle control, respectively, such as [16]–[19]. More specifically, different approaches are applied to the traffic signal optimization layer, in which the brutal force-based method is widely used, as can be seen in [16]–[18]. In the vehicle control layer, CAVs are usually grouped and controlled as stationary platoons, as such instead of optimizing the trajectories of all vehicles in the platoon, only the trajectory of the leader is controlled [16], [17], [20]. In contrast, [21] deals with a one-layer signal-vehicle control structure to simultaneously optimize traffic signals and vehicle trajectories at an isolated intersection. To mitigate the complexity of the single-layer problem, [21] formulates the joint optimal control problem (OCP) as a mixed integer linear program by linearizing the red phase logic constraints and the objective function of comfort and traffic delay. Nevertheless, the above methods mostly address fully automated scenarios of pure CAVs.

The mixed traffic scenario has recently received more attention [22]–[33]. Some of these works use an integrated optimization framework to jointly control signal timing and vehicle trajectory, such as [22]–[24]. For instance, in [24], multi-objective mixed-integer non-linear programming is established to optimize signal timing and vehicle trajectories. This aims to reduce stops at the traffic light and overall delays. Lagrangian relaxation is applied to decompose the original problem into separated lane-level submodels for reduced complexity. Nevertheless, the computational burden remains high for such joint optimization schemes due to the scale of the problem [34], [35]. In this context, the hierarchical control/optimization architecture emerges as a promising solution, where, in most cases, signal timing is optimized in the first place, followed by the vehicle trajectory control subject to the timing and phase plans from in the upper layer [25], [26]. More specifically, in [25], the signal phase duration is optimized to minimize total delay in the upper layer based on the fundamental diagram model of mixed traffic flow, which embeds CAV penetration rate and stable space headway. Next, the intersection arrival time of all CAVs is determined by finding their individual speed profiles by empirical rules. In [27], a joint traffic signal and vehicle speed rolling-horizon optimization method is introduced. It uses CAV data to determine the best signal timing and phasing plans, and then offers speed recommendations to each vehicle to reduce the total stops. This takes into account the possible response delay of the HDVs. Recently, [28] proposed a new scheduling method by introducing an additional "white signal phase", during which connected vehicles are forced to keep up with the vehicle immediately ahead to pass the intersection as a platoon. The optimization problem is formulated as a mixed-integer non-linear program linearized and incorporated into a receding horizon framework to tackle the complexities. In addition to model-based methods, promising results have been shown using data-driven and learning-based methods [36], [37] in the context of vehicle and traffic efficiency. However, the performance of this learning-based method is largely affected by the quality of training data [38].

The existing methods are mainly designed for maximizing travel time (represented by throughput, delay, and stops) whereas energy efficiency is either omitted or taken into account through conventional fuel consumption. As travel time and energy efficiency usually lead to contradicting optimal solutions, this paper investigates the trade-off between intersection throughput and the energy efficiency of all vehicles by co-optimizing the traffic SPAT and CAV trajectories (whereby the velocities of HDVs are indirectly governed following the notation of "$1 + N$" mixed platoon [39], [40]). Instead of using further alternative signal phases to promote CAV-led platoons (like [28]), the platoon formation is enforced by trajectory optimization in the present work. We examined how including electric vehicles (EVs) affects energy efficiency and compared it to scenarios with only conventional vehicles. To avoid solving a complex joint optimization problem that is computationally demanding, a two-layer control architecture is designed, respectively, for finding the SPAT and vehicle speed plans. The contributions of the paper are as follows:

1) In contrast to the majority of existing SPAT control solutions that rely on macroscopic traffic flow models [11], [28], [41], [42], the proposed solution makes use of microscopic vehicle motion and queue discharging models instead. Therefore, the control solution tends to be more responsive to the time-varying traffic demands at a road intersection.
2) A novel signal-vehicle coupled optimal control strategy is proposed for mixed platoons, which can find the trade-off between the two key metrics: traffic throughput and vehicle energy consumption, unlike most of the existing methods, which solely focus on one aspect.
3) The benefit of the newly developed method is shown by comparisons with various traditional strategies. Additionally, the impacts of intersection traffic density, flow distribution, and the penetration rates of CAV and EV are investigated by comprehensive simulation trials.

The remainder of this paper is organized as follows. Section II introduces the problem and the intersection model. The mixed platoon-based hierarchical control framework entailing the mixed platoon model, traffic SPAT optimization and speed trajectory optimization is presented in Section III. Simulation results and discussion are shown in Section IV. Finally, concluding remarks are given in Section V.

Notation: Let $\mathbb{R}$, $\mathbb{R}_{\geq 0}$, $\mathbb{R}_{>0}$, $\mathbb{N}$ and $\mathbb{N}_{>0}$ denote the real, the non-negative real, the strict positive real sets of numbers, natural numbers, and non-zero natural numbers, respectively. Given a vector $\mathbf{x} \in \mathbb{R}^n$, we will denote as $||\mathbf{x}||$ the Euclidean norm of $\mathbf{x}$. Given an arbitrary set $\mathcal{N}$, $|\mathcal{N}|$ defines the cardinality of the set.

II. Signalized Intersection Model

As illustrated in Fig 1, this paper considers a signalized road intersection with mixed traffic flow of CAVs and HDVs. The intersection layout studied in this work consists of two single-lane perpendicular and flat roads. The center of the intersection is the *Merging Zone* (MZ). Outside the MZ is the *Control Zone* (CZ), where the motion of each CAV can be fully controlled by a central intersection controller (IC). In addition, the IC is also responsible for manipulating the intersection traffic SPAT to maximize the intersection traffic throughput and vehicle energy efficiency. The lengths of the CZ and MZ are L_{CZ} and L_{MZ}, respectively. In this framework, the IC is responsible for manipulating both the traffic SPAT and the trajectories of the CAVs to maximize the intersection traffic throughput and vehicle energy efficiency. Further from the center, there is a *Communication Zone* (ComZ), in which

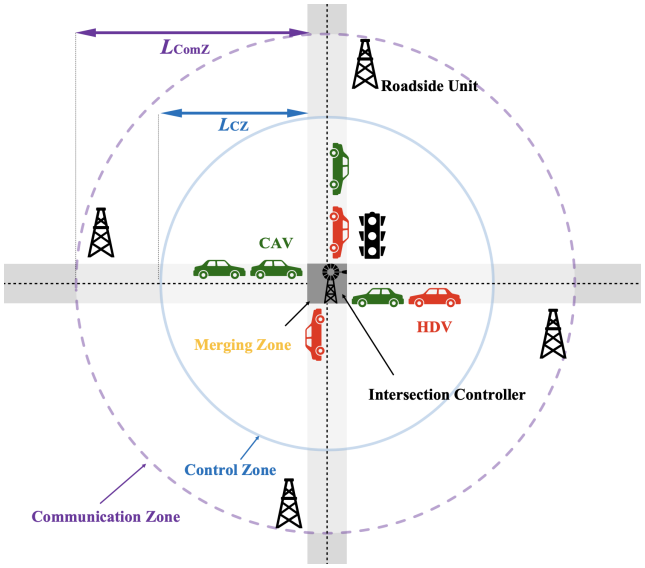

Fig. 1. The system architecture of a signalized four-way road intersection problem with consideration of mixed traffic flow of CAVs and HDVs. This single-lane scenario can be easily extended into multi-lane scenarios, although still in the context of no turning and no lane changing.

the IC can communicate with the CAVs. Moreover, there exist roadside units and sensors (camera, loop detector, etc.) at the entry points of the ComZ, where the entry speed, time, and length of the vehicles are measured and shared with the IC. For simplicity, turning is not considered in this framework while lane changes are only allowed outside the CZ. This may involve introducing an additional zone (centered at the intersection) beyond the control zone, where vehicles are allowed to perform lane changes in line with their turning intentions [43]. As such, the control design for lane changes may be decoupled from the control design for the intersection crossing (as addressed in the present paper). Fig. 2 shows a

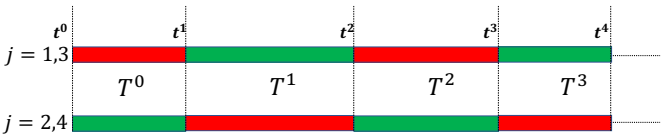

Fig. 2. Graphical representation of signal cycles.

graphical representation of a typical signal cycle for every approach at the intersection. In each phase the signal indicator is either green or red, while the amber phase is integrated into the red phase for safety purposes. Let $I_j^q \in \{0,1\}$ be the signal indicator at the qth ($q \in \mathbb{N}$) phase for the jth direction with $j \in \mathcal{J} = \{1,2,3,4\}$, which collects the four approaches of the intersection, with $\{1,3\}$ perpendicular to $\{2,4\}$. $I_j^q = 1$ is the green light and $I_j^q = 0$ is the red light. For the sake of further discussion, let $\mathcal{S}_j^q$ be the SPAT information set at the qth phase for the jth direction, it is defined as:

$$\mathcal{S}_j^q = \{T^q, I_j^q\},\ q \in \mathbb{N} \tag{1}$$

where $\mathcal{S}_j^0 = \{T^0, I_j^0\}$ is the predefined initial condition and T^q is the time duration of the qth signal phase. Then, let

$$t^q = t^0 + \sum_{k=0}^{q-1} T^k \tag{2}$$

be the start time of the qth SPAT provided t^0 is the initial time. The signal indication of the two perpendicular roads in this work are always reversed, and therefore, when the SPAT is determined for one direction, the other is determined accordingly. To complete the intersection model, the following assumptions are also needed.

Assumption 1. *Each CAV can communicate with the IC without errors and delays once the vehicles enter the control zone.*

Assumption 2. *After entering the CZ, all CAVs are fully controllable and capable of precisely following the trajectories provided by the IC.*

Assumption 3. *The communication zone is large enough, such that any vehicle that enters the ComZ at a green phase will not reach the stop line within the same phase.*

Assumptions 1 and 2 are commonly used in existing works, such as [14], [27], [40]. In this context, the IC can be informed of the type (whether it is a CAV or HDV) and the length of each vehicle upon arrival at ComZ. Assumption 3 is added to enable the formulation such that the corresponding optimization problem (the algorithm will be introduced in Section III) does not depend on unknown information outside the ComZ. Given the maximum vehicle speed $v_{\max}$ at a road intersection and the upper time duration limit of a signal phase $T_{\max}$ chosen in the present work, it is straightforward to determine the appropriate radius of the ComZ (i.e., $L_{\text{ComZ}} \geq v_{\max} T_{\max}$ which may be realized by multi-hop communication), such that Assumptions 3 is satisfied. For instance, when $v_{\max} = 15$ m/s and $T_{\max} = 50$s, Assumption 3 holds if $L_{\text{ComZ}} \geq 750$ m.

III. Mixed Platoon-based Signal-Vehicle Coupled Coordination Scheme

To address the signalized intersection coordination problem with mixed autonomy vehicles as illustrated in Fig. 1, this paper exploits the notion of the "$1+N$" mixed platoon where "1" represents the CAV leading a platoon and "N" collects the following HDVs with $N \in \mathbb{N}$. In particular, when $N = 0$, it represents a platoon with only a single CAV. As such, any mixed traffic flow can be decoupled into multiple mixed platoons with individual CAV leads. The mixed platoon model will be introduced in Section III-A, followed by the proposed signal-vehicle coupled control algorithm that is based on the concept of mixed platoons. The control algorithm follows a hierarchical architecture, where the upper layer is the traffic SPAT controller (see Section III-B) and the lower layer is the speed trajectories controller of CAVs (while the HDVs are indirectly controlled). The two layers are respectively presented in Section III-B and Section III-C. The overall control scheme is sketched in Fig. 3. The upper-level is designed to find the optimal light duration for the next phase T^{q*}, the number of mixed platoons allowed to cross the intersection within the phase l_j^{q*} and the target equilibrium speed (i.e., crossing speed) of the mixed platoons v_j^{q*} in terms of maximizing the intersection throughput. Note that a single v_j^{q*} is used for all crossing platoons to avoid rear-end collision between platoons. Then, at the lower-level, the optimal speed trajectories of each CAV are determined according to T^{q*}, l_j^{q*}, v_j^{q*} obtained at the upper-level so as to minimize the control effort of all each mixed platoon.

Before the introduction of the upper-level SPAT optimization, some preliminaries are introduced first. Let us consider $\mathcal{J}_1 = \{j \mid I_j^q = 1, \forall q \in 2\mathbb{N}+1\}$ and $\mathcal{J}_2 = \{j \mid I_j^q = 0, , \forall q \in 2\mathbb{N}+2\}$ with $\mathcal{J} = \mathcal{J}_1 \cup \mathcal{J}_2$. Without loss of generality, in the rest of Section III we assume $q \in 2\mathbb{N}+1$ in the proposed method, although the method can be easily applied to $q \in 2\mathbb{N}+2$. Let the set $\mathcal{V}^q$ represent the set of all vehicles inside the ComZ at $t = t^q$, then $\mathcal{V}^q = \cup_{j\in\mathcal{J}} \mathcal{V}_j^q$ where $\mathcal{V}_j^q$ collects the vehicles in direction j. The set $\mathcal{V}_j^q, \forall j \in \mathcal{J}_1$ is formed by the remaining vehicles $\tilde{\mathcal{V}}_j^q$ after the last green phase $t \in (t^{q-2}, t^{q-1}], \forall q \geq 2$ and the vehicles $\bar{\mathcal{V}}_j^q$ arriving at the ComZ during the subsequent red phase $t \in (t^{q-1}, t^q]$. Note that $\tilde{\mathcal{V}}_j^1, j \in \mathcal{J}_1$ represents the vehicles in the ComZ at $t = t^0$ that is predefined. With reference to the $1+N$ mixed platoon model, $\bar{\mathcal{V}}_j^q$ can be decomposed into multiple CAV-led mixed platoons and some HDVs ahead of the first CAV, such that $\bar{\mathcal{V}}_j^q = \mathcal{H}_j^q \cup_{l\in\bar{\mathcal{L}}_j^q} \mathcal{P}_{l,j}^q$, where $\mathcal{H}_j^q$ is the set of HDVs ahead of the first CAV in $\bar{\mathcal{V}}_j^q$ and $\mathcal{H}_j^q = \emptyset$ if the first element in $\bar{\mathcal{V}}_j^q$ is a CAV, $\mathcal{P}_{l,j}^q = \{1, 2, \ldots, |\mathcal{P}_{l,j}^q|\}$ the set of lth mixed platoon vehicles in $\bar{\mathcal{V}}_j^q$ and $\bar{\mathcal{L}}_j^q = \{1, 2, \cdots \bar{l}_j^q\}$ is the set of mixed platoons with the maximum platoon number denoted by $\bar{l}_j^q$. By combining the uncontrollable HDVs $\mathcal{H}_j^q$ with the awaiting vehicles $\tilde{\mathcal{V}}_j^q$ and letting $\mathcal{P}_{0,j}^q = \mathcal{H}_j^q \cup \tilde{\mathcal{V}}_j^q$, we have $\mathcal{V}_j^q = \cup_{l\in\mathcal{L}_j^q} \mathcal{P}_{l,j}^q$ with $\mathcal{L}_j^q = 0 \cup \bar{\mathcal{L}}_j^q$. Finally, $\mathcal{V}_j, \forall j \in \mathcal{J}_2$ only collects the residual vehicles after the green phase $t \in (t^{q-1}, t^q]$, thus $\mathcal{P}_{0,j}^q = \mathcal{V}_j, \forall j \in \mathcal{J}_2$. For ease of notation, one sets $n_{l,j}^q = |\mathcal{P}_{l,j}^q|$ that is the number of vehicles involved in a platoon $\mathcal{P}_{l,j}^q$.

A. Modeling of a mixed platoon system

The following assumption is invoked to model the mixed platoon system.

Assumption 4. *The motion of the HDVs can be characterized by the intelligent driver model (IDM) car-following model.*

For the sake of further analysis, let us denote $p_{l,i,j}^q(t)$, $v_{l,i,j}^q(t)$ and $a_{l,i,j}^q(t)$ respectively the (front-end) position, velocity and acceleration of the ith vehicle within the lth mixed platoon approaching from the direction j during qth signal phase. In particular, $p_{l,i,j}^q = 0$ refers to the entry point of the ComZ. Under Assumption 4, the acceleration of each HDV can be expressed as

$$\dot{a}_{l,i,j}^q(t) = F\left(s_{l,i,j}^q(t), \dot{s}_{l,i,j}^q(t), v_{l,i,j}^q(t)\right). \tag{3}$$

where $F\left(s_{l,i,j}^q(t), \dot{s}_{l,i,j}^q(t), v_{l,i,j}^q(t)\right)$ is a nonlinear function of the following distance $s_{l,i,j}^q(t) = p_{l,i-1,j}^q(t) - p_{l,i,j}^q(t)$ and the velocity difference $\dot{s}_{l,i,j}^q(t) = v_{l,i-1,j}^q(t) - v_{l,i,j}^q(t)$ between the preceding vehicle $i-1$ and the vehicle i. More specifically, $F\left(s_{l,i,j}^q(t), \dot{s}_{l,i,j}^q(t), v_{l,i,j}^q(t)\right)$ is defined as:

$$\begin{aligned} &F\left(s_{l,i,j}^q(t), \dot{s}_{l,i,j}^q(t), v_{l,i,j}^q(t)\right) \\ &= a_{\max}\left(1 - \left(\frac{v_{l,i,j}^q(t)}{v_d}\right)^{\delta} - \left(\frac{s_d\left(v_{l,i,j}^q(t), \dot{s}_{l,i,j}^q(t)\right)}{s_{l,i,j}^q(t)}\right)^2\right) \end{aligned} \tag{4}$$

where $a_{\max}$ is the maximum vehicle acceleration, δ is the acceleration exponent and v_d is the desired constant following velocity of an individual HDV. In the present paper, $\delta = 4$ and $v_d = v_{\max}$ are utilized, which are common choices in the literature to represent realistic driving behavior [44]. s_d is the desired distance headway of a human driver

$$s_d\left(v_{l,i,j}^q(t), \dot{s}_{l,i,j}^q(t)\right) = s_0 + v_{l,i,j}^q(t)T_0 - \frac{v_{l,i,j}^q(t)\dot{s}_{l,i,j}^q(t)}{2\sqrt{a_{\max}a_b}} \tag{5}$$

with s_0 the standstill spacing between consecutive vehicles, a_b the comfortable deceleration of each HDV, and T_0 the safe time headway.

It is worth remembering that HDVs are not controllable. Conversely, CAVs are fully controllable, and their longitudinal motion is modeled by a commonly used third-order model [45]:

$$\begin{cases} \dot{p}_{l,1,j}^q(t) = v_{l,1,j}^q(t), \\ \dot{v}_{l,1,j}^q(t) = a_{l,1,j}^q(t), \\ \dot{a}_{l,1,j}^q(t) = \dfrac{1}{\tau_{l,j}^q}u_{l,j}^q(t) - \dfrac{1}{\tau_{l,j}^q}a_{l,1,j}^q(t) \end{cases} \tag{6}$$

where $\tau_{l,j}^q$ and $u_{l,j}^q(t)$ are the inertial time-lag and the control input of the lth platoon leading CAVs in approach j of the qth phase, respectively. As it can be noticed, the heterogeneity of CAVs can be taken into account by $\tau_{l,j}^q$, which can be shared with the IC when the CAV enters the ComZ.

Considering v_j^{q*} the equilibrium speed of the mixed platoon and s_j^{q*} the equilibrium following distance, it holds that

$$\dot{v}_{l,i,j}^q = F\left(s_j^{q*}, 0, v_j^{q*}\right) = 0. \tag{7}$$

By introducing the error variables $\tilde{s}_{l,i,j}^q(t) = s_{l,i,j}^q(t) - s_j^{q*}$ and $\tilde{v}_{l,i,j}^q(t) = v_{l,i,j}^q(t) - v_j^{q*}$, the IDM model for an HDV (3)-(4) can be linearized around the equilibrium point, leading to

$$\begin{cases} \dot{\tilde{s}}_{l,i,j}^q(t) = \tilde{v}_{l,i-1,j}^q(t) - \tilde{v}_{l,i,j}^q(t), \\ \dot{\tilde{v}}_{l,i,j}^q(t) = \alpha_1\tilde{s}_{l,i,j}^q(t) - \alpha_2\tilde{v}_{l,i,j}^q(t) + \alpha_3\tilde{v}_{l,i-1,j}^q(t) \end{cases} \tag{8}$$

where $\alpha_1 = \frac{\partial F}{\partial s_{l,i,j}^q}, \alpha_2 = \frac{\partial F}{\partial \dot{s}_{l,i,j}^q} - \frac{\partial F}{\partial v_{l,i,j}^q}, \alpha_3 = \frac{\partial F}{\partial \dot{s}_{l,i,j}^q}$ evaluated at the equilibrium state (v_j^{q*}, s_j^{q*}).

Consider an arbitrary mixed platoon $\mathcal{P}_{l,j}^q$ (which involves $n_{l,j}^q - 1$ HDV followers by definition). By combining the system equations (6) and (8) for all $n_{l,j}^q$ vehicles within the mixed platoon, the mixed platoon system can be recast into a single state-space model:

$$\dot{x}_{l,j}^q(t) = A_{l,j}^q x_{l,j}^q(t) + B_{l,j}^q u_{l,j}^q(t) \tag{9}$$

where the aggregated state and input vectors are

$$\begin{aligned} x_{l,j}^q(t) = \Big[&p_{l,1,j}^q(t),\, v_{l,1,j}^q(t),\, a_{l,1,j}^q(t),\, \tilde{s}_{l,2,j}^q(t), \tilde{v}_{l,2,j}^q(t), \\ &\tilde{s}_{l,3,j}^q(t), \tilde{v}_{l,3,j}^q(t),\, \ldots,\, \tilde{s}_{l,n_{l,j}^q-1,j}^q(t), \tilde{v}_{l,n_{l,j}^q-1,j}^q(t)\Big]^\top \\ &\in \mathbb{R}^{2n_{l,j}^q+1}. \end{aligned} \tag{10}$$

and $A_{l,j}^q \in \mathbb{R}^{(2n_{l,j}^q+1)\times(2n_{l,j}^q+1)}$ and $B_{l,j}^q \in \mathbb{R}^{(2n_{l,j}^q+1)}$ are given as follows

$$A_{l,j}^q = \begin{bmatrix} A_{l,1} & 0 & \ldots & \ldots & 0 & 0 \\ H_2 & H_1 & 0 & \ldots & \ldots & 0 \\ 0 & H_2 & H_1 & 0 & \ldots & 0 \\ \vdots & \ddots & \ddots & \ddots & \ddots & \vdots \\ 0 & \ldots & 0 & H_2 & H_1 & 0 \\ 0 & \ldots & \ldots & 0 & H_2 & H_1 \end{bmatrix}, \tag{11}$$

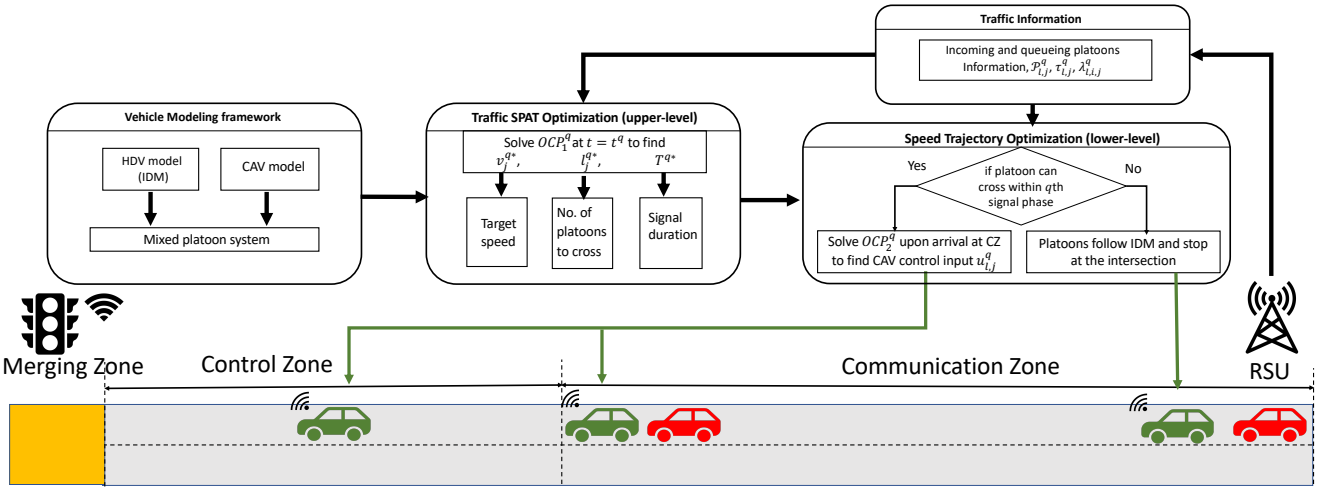

Fig. 3. The scheme of the hierarchical mixed platoon control framework with traffic SPAT optimization and speed trajectory optimization for the signalized mixed intersection problem sketched in Fig. 1. CAVs and HDVs are represented by green and red vehicles, respectively. The optimization problems in upper and lower level are formulated in (24) and (35), respectively. Note that HDVs are not controlled and they always follow IDM with $v_d = v_{\max}$ (3).

$$B_{l,j}^q = \begin{bmatrix} 0 & 0 & \dfrac{1}{\tau_{l,j}} & 0 & 0 & \dots & 0 \end{bmatrix}^\top, \tag{12}$$

with

$$A_{l,1} = \begin{bmatrix} 0 & 1 & 0 \\ 0 & 0 & 1 \\ 0 & 0 & -\frac{1}{\tau_{l,j}} \end{bmatrix}, H_1 = \begin{bmatrix} 0 & -1 \\ \alpha_1 & -\alpha_2 \end{bmatrix}, H_2 = \begin{bmatrix} 0 & 1 \\ 0 & \alpha_3 \end{bmatrix}. \tag{13}$$

The controllability of the mixed platoon system (9) is characterized by the following Lemma [40].

Lemma III.1. *The $1+N$ mixed platoon system is controllable when the following condition holds*

$$\alpha_1 - \alpha_2\alpha_3 + \alpha_3^2 \neq 0 \tag{14}$$

B. Traffic SPAT planner

In the SPAT optimization, vehicles belonging to $\mathcal{P}_{0,j}^q$ are assumed static, and it yields a queue of $n_{0,j}^q$ vehicles ahead of the $\bar{l}_j^q$ platoons. In the following, we denote by $\lambda_{l,i,j}^q$ the length of the ith vehicle in $\mathcal{P}_{l,j}^q$. The objective of the SPAT optimization is to minimize the total waiting time of all vehicles. The waiting time $T_{l,j}^{wait}$ of a vehicle in the lth mixed platoon to enter the MZ can be evaluated for all $l \in \mathcal{L}_j^q$ by:

$$T_{l,j}^{q,wait} = \begin{cases} T^{q*} - \hat{T}_{l,j}^{q,stop}, & \text{if } j \in \mathcal{J}_2, \\ \beta_{l,j}^q (T^{q*} + \hat{T}^{q+1} - \hat{T}_{l,j}^{q,stop}), & \text{if } j \in \mathcal{J}_1, \end{cases} \tag{15}$$

where $\hat{T}_{l,j}^{q,stop}$ is the minimum time required for lth platoon to reach the stop line

$$\hat{T}_{l,j}^{q,stop} = \frac{L_{\text{ComZ}} - p_{l,1,j}^q(t^q)}{v_{\max}}$$

The elimination of $\hat{T}_{l,j}^{q,stop}$ is motivated by the fact that the initial distance to the stop line of a platoon is an indispensable part of the mission regardless of the crossing decision. In addition, $\beta_{l,j}^q$ is a binary indicator given by

$$\beta_{l,j}^q = \begin{cases} 0, & \text{if } l \leq l_j^{q*}, \\ 1, & \text{if } l > l_j^{q*}, \end{cases} \tag{16}$$

where $\beta_{l,j}^q = 0$ represents platoon l can complete the intersection crossing during the qth green signal light phase. Conversely, $\beta_{l,j}^q = 1$ is the case that the platoon cannot pass through the intersection within the current phase and has to wait for another red phase T^{q+1}. $\hat{T}^{q+1}$ is the estimate of T^{q+1}, and is approximated by the prior red light duration time, $\hat{T}^{q+1} = T^{q-1}$, when evaluating the waiting time in the SPAT optimization (24), which is compatible with the traffic flow that does not change suddenly.

To determine the number of vehicles that can pass through the intersection, the queue discharge time at the intersection needs to be estimated. The initial distance (at $t = t^q$) from the rear end of the last vehicle in the queue $\mathcal{P}_{0,j}^q$ to the exit of the MZ is defined as $D_{0,j}^q$, which is calculated by

$$D_{0,j}^q = L_{\text{MZ}} + \sum_{i=1}^{n_{0,j}^q} \left(\lambda_{0,i,j}^q + s_0\right) - s_0 \tag{17}$$

For computational efficiency of the prediction, when the traffic signal turns to green indication, we simply assume that all the vehicles in the queue follow a constant acceleration a_d ($a_d \leq a_{\max}$) until $v_{\max}$ is reached, where $v_{\max}$ is the maximum speed limit. Being a_d a tuneable parameter, it is possible to design a suitable a_d to ensure safety and comfort [46]. In this context, the time required for the last vehicle in the queue to leave the MZ can be estimated by:

$$T_{n_j^q} = \begin{cases} \displaystyle\sum_{i=1}^{n_{0,j}^q} \kappa_{0,i,j}^q + \frac{\sqrt{2a_d D_{0,j}^q}}{a_d} & \text{if } D_{0,j}^q \leq \dfrac{v_{\max}^2}{2a_d} \\ \displaystyle\sum_{i=1}^{n_{0,j}^q} \kappa_{0,i,j}^q + \frac{v_{\max}}{a_d} + \frac{D_{0,j}^q - \frac{v_{\max}^2}{2a_d}}{v_{\max}} & \text{otherwise} \end{cases} \tag{18}$$

where $\kappa_{0,i,j}^q$ represents the anticipated response delay of a human driver. Therefore, $\kappa_{0,i,j}^q = \kappa_0$ when the queueing vehicle i is an HDV and $\kappa_{0,i,j}^q = 0$ in the case of a CAV, with $\kappa_0 \in \mathbb{R}_{>0}$ being a tunable parameter.

To ensure that the first mixed platoon $\mathcal{P}_{1,j}^q$, $j \in \mathcal{J}_1$ does not (rear-end) collide with the last vehicle in the discharge queue

and to maximize the traveling speed of all platoons, the target crossing speed v_j^{q*} of the first platoon is set to

$$v_j^{q*} = \min\left(v_{\max}, \frac{L_{\text{ComZ}}+L_{\text{MZ}}-p_{1,1,j}^q(t^q)}{T_{n_j^q}}\right) \tag{19}$$

which is then utilized for all platoons allowed to cross during the qth phase for safety consideration as the movement of the remaining platoons is constrained by the first one. The length of the lth mixed platoon, $D_{l,j}^q$, at steady state with target velocity v_j^{q*} can be determined by

$$D_{l,j}^q = \sum_{i=1}^{n_{l,j}^q}\left(\lambda_{l,i,j}^q + s_j^{q*}\right) \tag{20}$$

where the steady state headway s_j^{q*} can be expressed as a function of v_j^{q*} owing to (7), as given by:

$$s_j^{q*} = \frac{s_0 + v_j^{q*}T_0}{\sqrt{1-\left(v_j^{q*}/v_{\max}\right)^4}}. \tag{21}$$

The SPAT optimization aims to find the optimal signal phase T^{q*} that allows a certain number of mixed platoons l_j^{q*}, $j \in \mathcal{J}_1$ to cross the intersection. To this end, let us define $T_{\min,l,j}^q$ the minimum time required for the entire lth platoon to pass the intersection. It can be represented as a function of v_j^{q*}, as follows:

$$T_{\min,l,j}^q = \begin{cases} T_{n_j^q}, & l=0 \\ \dfrac{L_{\text{ComZ}}+L_{\text{MZ}}-p_{l,1,j}^q+D_{l,j}^q}{v_j^{q*}}, & l \in \bar{\mathcal{L}}_j^q \end{cases} \tag{22}$$

where $j \in \mathcal{J}_1$. It is evident that a platoon l can cross the intersection if $T_{\min,l,j}^q \le T_{\max}$. For the sake of further discussion, consider $\mathcal{L}_{j,f}^q = \{l \mid T_{\min,l,j}^q \le T_{\max}, j \in \mathcal{J}_1\} \subset \mathbb{N}$ the feasible set of platoons that could potentially cross the intersection within the upcoming green phase. Furthermore, given the optimal number of platoons that are allowed to cross the intersection in both green phase directions, l_j^{q*}, $j \in \mathcal{J}_1$ and the resulting $T_{\min,l,j}^{q*}$ by (22), the optimal signal phase duration is defined by

$$T^{q*} = \max_{j\in\mathcal{J}_1}(T_{\min,l,j}^{q*}) \tag{23}$$

We now have all ingredients to formulate the upper-level SPAT optimization, which has now been reduced to find the optimal number of crossing platoons l_j^{q*}, $j \in \mathcal{J}_1$ so as to minimize the total waiting time of all vehicles approaching from the four directions for each traffic signal cycle. This leads to an integer programming problem:

$$\mathcal{OCP}_1^q : \min_{l_j^{q*}\in\mathcal{L}_{j,f}^q} \quad \sum_{j\in\mathcal{J}}\sum_{l\in\mathcal{L}_j^q} n_{l,j}^q T_{l,j}^{q,wait} \tag{24}$$

where $T_{l,j}^{q,wait}$ can be determined by (15)-(23) utlizing T^{q*} determined by (23). The minimum solution of problem $\mathcal{OCP}_1^q$ can be found by searching over the space $\mathcal{L}_{j,f}^q$.

Remark 1. *The optimization problem* (24) *may be infeasible if there does not exist a T^{q*} (following* (23)*) that satisfies the constraint $[0, T_{\max}]$ (e.g., the initial waiting queue $\mathcal{P}_{0,j}^q$ is extremely long, which implies heavy traffic). In such a circumstance, the optimal phase duration follows $T^{q*} = T_{\max}$.*

C. Speed trajectory controller

Given the optimal v_j^{q*}, T^{q*}, l_j^{q*} determined at the upper-level, the aim of the speed trajectory planning at the lower level is to ensure that the vehicles in $\mathcal{P}_{l,j}^q$ can efficiently form a mixed platoon at the steady state velocity v_j^{q*} and complete the intersection crossing within the time duration T^{q*} of the green signal light phase if $l \le l_j^{q*}$ or otherwise stop properly.

Let us first focus on the platoons $l \le l_j^{q*}$ that are permitted to cross within the qth signal phase. According to Assumption 3, the optimal decisions v_j^{q*}, T^{q*}, l_j^{q*} are not available when a mixed platoon $\mathcal{P}_{l,j}^q$ enters the ComZ. To facilitate the platoon control inside the CZ, the IC will suggest each leading CAV of a platoon that has not yet entered the CZ a target velocity, $\hat{v}_{l,j}^{q*}$, and the movement of those CAVs will be governed by IDM as with uncontrolled HDVs.

With the aim of maximizing the throughput and avoiding rear-end collisions, $\hat{v}_{l,j}^{q*}, \forall l \in \tilde{\mathcal{L}}_j^q$ is calculated by:

$$\hat{v}_{l,j}^{q*} = \min\left(v_{\max}, \frac{L_{\text{ComZ}}+L_{\text{MZ}}}{\hat{t}_{l,j}^q - \tilde{t}_{l,j}^q}\right) \tag{25}$$

where $\tilde{t}_{l,j}^q$ is the ComZ entering time of the platoon $\mathcal{P}_{l,j}^q$ and $\hat{t}_{l,j}^q$ is the estimated arriving time of the lead vehicle of the lth platoon at the exit point of the MZ. $\hat{t}_{l,j}^q$ is estimated by

$$\hat{t}_{l,j}^q = \begin{cases} t^q + \hat{T}_{0,n_j^q}, & l=1 \\ \hat{t}_{l-1,j}^q + \hat{T}_{l-1,n_j^q}, & l \in \bar{\mathcal{L}}_j^q \backslash 1 \end{cases} \tag{26}$$

where $\hat{T}_{l-1,n_j^q}$ is the estimated discharging time required for the $(l-1)$th platoon, which is determined as follows:

$$\hat{T}_{l-1,n_j^q} = \begin{cases} T_{n_j^q}, & l=1, \\ \dfrac{\sum_{i=1}^{n_{l-1,j}^q}\left(\lambda_{l-1,i,j}^q + \hat{s}_{l-1,j}^{q*}\right) - \hat{s}_{l-1,j}^{q*}}{\hat{v}_{l-1,j}^{q*}}, & \text{otherwise}, \end{cases} \tag{27}$$

where $T_{n_j^q}$ is the queue discharging time defined in (18), $\hat{s}_{l,j}^{q*}$ is the steady state headway associated with $\hat{v}_{l,j}^{q*}$, determined by (21). In view of (25)-(27), given $T_{n_j^q}$, then $\hat{T}_{l-1,n_j^q}$, $\hat{t}_{l,j}^q$ and $\hat{v}_{l,j}^{q*}$ can be recursively determined for each l.

For every platoon entering the CZ, the IC optimizes its trajectory by solving an individual OCP (for the speed trajectory optimization) based on v_j^{q*}, T^{q*} and l_j^{q*} from the upper layer obtained at t^q. Consider $\bar{t}_{l,j}^q$ the CZ entering time of the platoon $\mathcal{P}_{l,j}^q$. For the sake of further discussion, let us denote $\tilde{\mathcal{L}}_j^q = \{l | \bar{t}_{l,j}^q \ge t^q\}$ the index of platoons that can be informed of the target speed v_j^{q*} and the signal phase T^q by the upper-level SPAT planner upon arrival at the CZ. Then, $\bar{\mathcal{L}}_j^q \backslash \tilde{\mathcal{L}}_j^q$ represents the platoons which enter the CZ before t^q, and therefore can not be informed. In this framework, the lower-level speed trajectory optimization is activated at $t = \bar{t}_{l,j}^q$ for $l \in \tilde{\mathcal{L}}_j^q$, while for $l \in \bar{\mathcal{L}}_j^q \backslash \tilde{\mathcal{L}}_j^q$, it is triggered at $t = t^q$, and for $t \in [\bar{t}_{l,j}^q, t^q)$ (when the mixed platoon is in the CZ but the results of upper-level optimization are not available), the leading CAV of each of those platoons will continue following the IDM with the target speed specified in (25). Before introducing the OCP for speed optimization, let us define the coordination constraints.

To avoid rear-end collisions between vehicles in a platoon, and the lead vehicle of the lth platoon and the last vehicle in its preceding platoon, the following collision avoidance constraints are enforced, respectively:

$$\tilde{s}^q_{l,i,j}(t) + s^{q*}_j \geq s_0 + v^q_{l,i,j}(t)T_0 \tag{28}$$

$$p^q_{l,1,j}(t) \leq p^q_{l-1,n^q_{l-1,j},j}(t) - (s_0 + v^q_{l,1,j}(t)T_0), \forall l \in \bar{\mathcal{L}}^q_j \tag{29}$$

Moreover, for safety purposes, the velocity of any vehicles and the control input of the leading CAV of any platoon are constrained by:

$$0 < v^q_{l,1,j} \leq v_{\max}, \tag{30a}$$
$$a_{\min} \leq a^q_{l,1,j} \leq a_{\max}, \tag{30b}$$
$$0 < \tilde{v}_{l,i,j}(t) + v^{q*}_j \leq v_{\max},\ i \in \mathcal{P}^q_{l,j}\backslash 1 \tag{30c}$$
$$u_{\min} \leq u^q_{l,j}(t) \leq u_{\max}, \tag{30d}$$

where $u_{\min}$ and $u_{\max}$ are the minimum and maximum CAV control input, respectively.

To ensure that the full body length of the last vehicle in a platoon (that is allowed to cross) can leave the MZ within the green phase, the following constraint is also required:

$$L_{\text{ComZ}} + L_{\text{MZ}} - \bar{p}^q_{l,n^q_{l,j},j} + \lambda^q_{l,n^q_{l,j},j} \leq d^q_{l,n^q_{l,j},j} \tag{31}$$

where $\bar{p}^q_{l,n^q_{l,j},j}$ is the position of the last vehicle in $\mathcal{P}^q_{l,j}$ when the speed optimization is triggered

$$\bar{p}^q_{l,n^q_{l,j},j} = \begin{cases} p^q_{l,n^q_{l,j},j}(\bar{t}^q_{l,j}), & l \in \tilde{\mathcal{L}}^q_j \\ p^q_{l,n^q_{l,j},j}(t^q), & l \in \bar{\mathcal{L}}^q_j \backslash \tilde{\mathcal{L}}^q_j \end{cases}$$

$\bar{p}^q_{l,n^q_{l,j},j}$ is available to the IC by vehicular communication if the vehicle is connected (CAVs and connected HDVs) or by prediction through IDM refer to Assumption 4 (unconnected HDVs). $d^q_{l,n^q_{l,j},j}$ is the total distance traveled by the last car in the platoon during the entire time horizon of the optimization, that is $[\bar{t}^q_{l,j},\ t^q_{f,l,j}]$ for $l \in \tilde{\mathcal{L}}^q_j$ and $[t^q,\ t^q_{f,l,j}]$ for $l \in \bar{\mathcal{L}}^q_j \backslash \tilde{\mathcal{L}}^q_j$ with $t^q_{f,l,j}$ the terminal (MZ exit) time of the lth platoon in jth direction and qth phase. Instead of enforcing a prescribed terminal time, which might be restrictive, in this work, a time slot for a platoon to leave the MZ is assigned (i.e., a constraint for the terminal time):

$$\begin{cases} t^q_{f,l,j} \in [\max(\underline{t}^q_{l,j}, t^q + T_{n^q_j}), \min(\bar{t}^q_{l,j}, t^q + T^{q*})], l = 1 \\ t^q_{f,l,j} \in [\max(\underline{t}^q_{l,j}, t^{q*}_{f,l-1,j}), \min(\bar{t}^q_{l,j}, t^q + T^{q*})], l > 1 \end{cases} \tag{32}$$

where $t^{q*}_{f,l,j}$ is the optimal terminal time for lth platoon and

$$\underline{\hat{t}}^q_{l,j} = \begin{cases} \dfrac{L_{\text{ComZ}} + L_{\text{MZ}} - \bar{p}^q_{l,n^q_{l,j},j} + \lambda^q_{l,n^q_{l,j},j}}{v_{\max}} + \bar{t}^q_{l,j}, & l \in \tilde{\mathcal{L}}^q_j \\ \dfrac{L_{\text{ComZ}} + L_{\text{MZ}} - \bar{p}^q_{l,n^q_{l,j},j} + \lambda^q_{l,n^q_{l,j},j}}{v_{\max}} + t^q, & l \in \bar{\mathcal{L}}^q_j \backslash \tilde{\mathcal{L}}^q_j \end{cases} \tag{33}$$

$$\bar{\hat{t}}^q_{l,j} = \begin{cases} \dfrac{L_{\text{ComZ}} + L_{\text{MZ}} - \bar{p}^q_{l,n^q_{l,j},j} + \lambda^q_{l,n^q_{l,j},j}}{\min(v^{q*}_j, \hat{v}^{q*}_{l,j})} + \bar{t}^q_{l,j}, & l \in \tilde{\mathcal{L}}^q_j \\ \dfrac{L_{\text{ComZ}} + L_{\text{MZ}} - \bar{p}^q_{l,n^q_{l,j},j} + \lambda^q_{l,n^q_{l,j},j}}{\min(v^{q*}_j, \hat{v}^{q*}_{l,j})} + t^q, & l \in \bar{\mathcal{L}}^q_j \backslash \tilde{\mathcal{L}}^q_j \end{cases} \tag{34}$$

Note that consideration of $t^q + T_{n^q_j}$, $t^{q*}_{f,l,j}$ and $t^q + T^{q*}$ can prevent overlaps between time slots and late MZ exit time ($> t^q + T^{q*}$), which may lead to infeasibility.

Now, we can formulate the OCP to optimize the trajectory of a platoon $\mathcal{P}^q_{l,j}$. The problem is given by

$$\mathcal{OCP}^q_2 : \min_{\mathbf{u}^q_{l,j}, t^q_{f,l,j}} W_1\|\mathbf{u}^q_{l,j}(t)\| + W_2\|\mathbf{v}^q_{l,j}(t) - v^{q*}_j\| + W_3\|\mathbf{s}^q_{l,j}(t) - s^{q*}_j\|, \tag{35a}$$
$$\textbf{s.t. } (9)-(13), (26)-(34) \tag{35b}$$
$$\textbf{given: } \bar{x}^q_{l,j}, v^{q*}_j, S^q_j, \mathcal{P}^q_{l,j} \tag{35c}$$

where $\mathbf{u}^q_{l,j}(t)$ is the control input of the leading CAV in the mixed platoon $\mathcal{P}^q_{l,j}$, $\mathbf{v}^q_{l,j}(t) = [v^q_{l,1,j}, v^q_{l,2,j}, ..., v^q_{l,n^q_{l,j},j}]^\top \in \mathbb{R}^{n^q_{l,j}}$ and $\mathbf{s}^q_{l,j}(t) = [s^q_{l,2,j}, s^q_{l,3,j}, ..., s^q_{l,n^q_{l,j},j}]^\top \in \mathbb{R}^{n^q_{l,j}-1}$ are stacked vectors of the velocity and inter-vehicle distance of each vehicle in the platoon $\mathcal{P}^q_{l,j}$ respectively. $\bar{x}^q_{l,j}$ is the initial condition of the platoon system (9), expressed as:

$$\bar{x}^q_{l,j} = \begin{cases} x^q_{l,j}(\bar{t}^q_{l,j}), & l \in \tilde{\mathcal{L}}^q_j \\ x^q_{l,j}(t^q), & l \in \bar{\mathcal{L}}^q_j \backslash \tilde{\mathcal{L}}^q_j \end{cases}$$

The objective function in (35a) is designed to minimize the control effort (which is loosely related to the energy consumption) and the deviations from the target speed v^{q*}_j and headway distance s^{q*}_j so that the platoon is formed. W_1, W_2 and W_3 are the weighting coefficients respective for the three objectives. The optimization problem (35) involves quadratic cost function and linear constants and can be solved efficiently by standard convex optimization tools.

During $[t^{q-1}, t^{q+1}]$, the platoons arriving at the ComZ after the l^{q*}_jth platoon are not permitted to cross the intersection within the qth signal phase. Conversely, they will form the waiting queue, $\mathcal{P}^{q+2}_{0,j}$, for the $(q+2)$th signal phase. In the proposed framework, these vehicles will be informed of the decision (at $t = t^q$ for platoons arriving at the ComZ before $t = t^q$ or upon arrival at the ComZ), and they will follow the IDM model subject to a desired velocity v_d to form the queue. In the proposed framework, v_d is set to $v_{\max}$ (as with the HDV model (4)) to conforms with the assumption – the queue $\mathcal{P}^q_{0,j}$ is static – imposed in the upper layer SPAT planner at the price of potentially increasing energy usage. Further optimal design of v_d corresponds to another optimization problem, which is beyond the scope of the present article. For instance, to avoid stops at the red light, v_d can be optimized by taking into account the present green and upcoming red phases (see, for example, [40]). Nevertheless, this could lead to an extremely small target velocity, thereby reducing the inflow speed at the intersection, and such a slow speed may not be preferred by human drivers.

Remark 2. *$\mathcal{OCP}^q_2$ may be infeasible due to the bi-level optimization structure. For example, the l^{q*}_jth platoon can not fully cross the intersection by the end of the green phase. To deal with this limitation, the first platoon that can not yield a feasible solution of $\mathcal{OCP}^q_2$ will be truncated by dropping the last HDV and re-solving $\mathcal{OCP}^q_2$. This will be repeated recursively until a feasible solution is found, and the truncated vehicles and platoons after that will be added to $\mathcal{P}^{q+2}_{0,j}$.*

IV. Simulation Validation

In this section, the performance of the proposed control framework is evaluated and compared with a recently proposed

coupled vehicle-signal control (CVSC) method [25] and two traditional benchmark methods in terms of traffic throughput and energy economy. In contrast to the proposed signal-vehicle co-control method, the two benchmark methods involve either SPAT or vehicle speed optimization only whereas the other layer in both methods is pre-defined, respectively. The two methods are defined below in Section IV-A followed by the introduction of the energy consumption model and the simulation environment. The impact of EV penetration rate on energy consumption is also studied. In addition, the impacts of traffic volume distribution across the perpendicular directions (i.e., either the same or different arrival rates of the horizontal directions from the vertical directions) and CAV penetration rate on the traffic energy economy and throughput are investigated.

A. Benchmark algorithms and comparison metrics

a) Fixed SPAT and Speed Optimization (F-SPAT): This benchmark method finds the optimal velocity trajectories of all vehicles by following the proposed lower-layer optimal control scheme (35) subject to a fixed (non-optimized) SPAT policy. Herein, the fixed SPAT follows a constant time duration for all signal phases, which is set to $T_{\max}/2$, the middle value of the time duration limits of a signal indication.

b) Optimized SPAT and IDM (O-SPAT): This method adopts the SPAT optimization algorithm (24) to find an optimized SPAT. However, the vehicle speed trajectories are not optimized. Instead, both CAVs and HDVs follow the IDM car-following model (4) with $v_d = v_{\max}$.

To fairly compare the eco-driving performance of all algorithms, the fuel consumption model developed in [47] is utilized for post-evaluation of the resulting traditional vehicles' energy usage of the speed trajectories in all algorithms. Considering a vehicle i in platoon $\mathcal{P}^q_{l,j}$, the fuel consumption rate of this vehicle $\phi^q_{l,i,j}$ (in milliliters per second) can be estimated by

$$\phi^q_{l,i,j} = b_0 + b_1 v^q_{l,i,j} + b_2 (v^q_{l,i,j})^2 + b_3 (v^q_{l,i,j})^3 + \hat{a}\left(c_0 + c_1 v^q_{l,i,j} + c_2 (v^q_{l,i,j})^2\right) \quad (36)$$

where $\hat{a}$ is the estimated "total" acceleration required by each vehicle to follow the specified speed trajectory, which includes the actual vehicle acceleration $a^q_{l,i,j}$ and the "acceleration" required to counterbalance friction forces due to the air drag and tire rolling resistances. Therefore, $\hat{a} = a^q_{l,i,j} + \frac{1}{2m} C_D \rho_a A_V (v^q_{l,i,j})^2 + \mu g$, where m is the vehicle mass, A_V is the vehicle frontal area, ρ_a is the air density, C_D and μ are air drag and tire rolling resistance coefficients, respectively. Note that the parameters A_V, C_D, μ, m are fixed (that represents a general-purpose car, see Table I) in the post-evaluation for simplicity. The fitting parameters in (37), (36) are $b_0 = 0.1569$, $b_1 = 2.450 \times 10^{-2}, b_2 = -7.415 \times 10^{-4}, b_3 = 5.975 \times 10^{-5}$, $c_0 = 0.07224, c_1 = 9.681 \times 10^{-2}$, and $c_2 = 1.075 \times 10^{-3}$, which are obtained by fitting the map of a 1.3L engine [47].

To study the influence EV penetration rate on the energy efficiency, the commonly used energy consumption (in watt) model for an electric drive is introduced:

$$\phi^q_{l,i,j} = e_1 m v^q_{l,i,j} a^q_{l,i,j} + e_2 (m a^q_{l,i,j})^2 \quad (37)$$

where $e_1 = 1.052 \times 10^{-3}, e_2 = 4.458 \times 10^{-7}$ are obtained by fitting the experimental data [3].

Eventually, the fuel/energy consumption of an individual vehicle is calculated by

$$\Phi^q_{l,i,j} = \int_{\mathcal{T}^q_{l,i,j}} \phi^q_{l,i,j} \mathrm{d}t, \quad (38)$$

where $\mathcal{T}^q_{l,i,j}$ is the time duration required by the vehicle to leave the MZ from the entry point of the ComZ, available once each vehicle leaves the MZ. By introducing the calorific value of the gasoline C_f, the fuel consumption (in milliliters) can be transformed into energy consumption (in KJ) for a fair comparison.

Without loss of generality, the control problem is initialized with randomized ComZ arrival conditions (time and speed for each vehicle), vehicle lengths and the inertial time-lags (only for CAVs, see (6)) in the following case studies. In particular, the inertial time-lags and the vehicle lengths are generated within suitable sets (see Table I), which can represent internal combustion engine vehicles with similar car dimensions so that the two parameters are compatible with the fuel consumption model (36) and its overall parameter choices. Moreover, the arrival (initial) speeds of the vehicles follow a uniform distribution within $(0, v_{\max}]$, while their arrival times follow a Poisson distribution. Finally, the vehicle and intersection parameters are summarized in Table I, and all simulation case studies are carried out in the Matlab environment.

TABLE I
VEHICLE AND INTERSECTION PARAMETERS

symbol	value	description
m	1200 kg	vehicle mass
T_0	0.5 s	safe time headway
s_0	1 m	standstill distance
$\lambda^q_{l,i,j}$	[4 m, 5 m]	car length
Δt	0.1 s	sampling time interval for vehicle
T_s	1 s	sampling time interval for IC
L_{CZ}	300 m	length of control zone
L_{ComZ}	750 m	length of communication zone
L_{MZ}	10 m	length of merging zone
$T_{\max}$	50 s	upper time limit of a signal light phase
$v_{\max}$	15 m/s	maximum velocity
$a_{\min}/a_{\max}$	$-6/4$ m/s^2	maximum deceleration and acceleration
a_d	3 m/s^2	acceleration of the discharging queue
a_b	-2 m/s^2	comfortable deceleration
$\tau^q_{l,i,j}$	[0.4, 0.7]	CAV inertial time-lag
A_V	2.5 m^2	vehicle frontal area
ρ_a	1.184 kg	air density
C_d	0.32	air drag coefficient
C_f	34.5 kJ/mL	calorific value of the gasoline
μ	0.015	tire rolling resistance coefficient
κ_0	0.7 s	response delay of a human driver
W_1	1000	Weighting parameter of $\mathcal{OCP}^q_2$
W_2, W_3	10	Weighting parameter of $\mathcal{OCP}^q_2$

B. Simulation Results

In the first instance, the proposed SPAT and vehicle co-control method is simulated in a scenario where the vehicle arrival rate in each direction (lane) is 1000 veh/h/lane (vehicles per hour per lane) with an overall penetration rate of CAV of 50%. The position trajectories of all vehicles (from the entry point of the CZ to the exit of the MZ) and the phases of the traffic signals are shown in Fig. 4. Note that for clarity of the figure, only two perpendicular approaches are shown here. As it can be seen, there are no rear-end (the position trajectories do not intersect each other) and lateral collisions (vehicles from the two perpendicular directions do not appear

This article has been accepted for publication in IEEE Transactions on Transportation Electrification. This is the author's version which has not been fully edited and content may change prior to final publication. Citation information: DOI 10.1109/TTE.2024.3394595

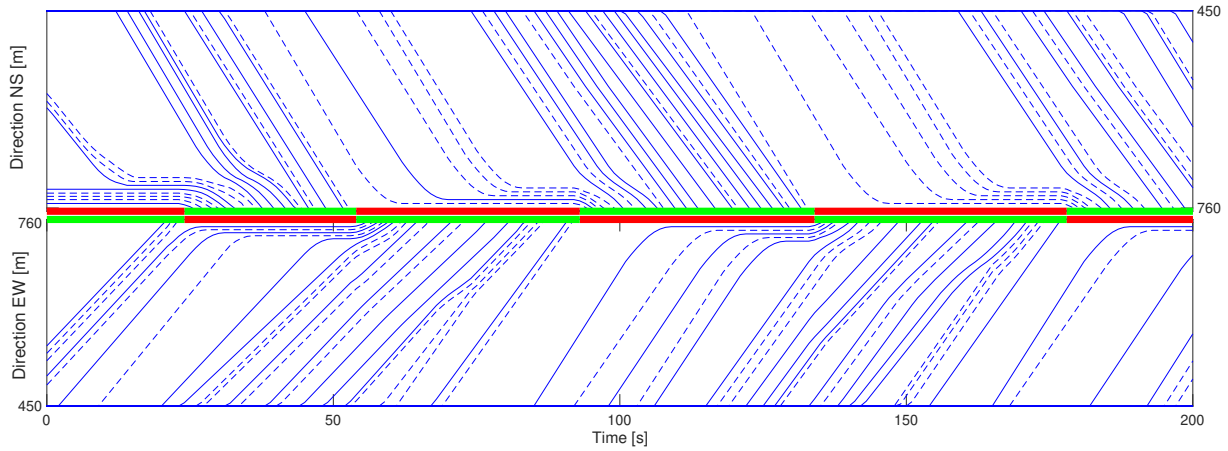

Fig. 4. Traffic SPAT and vehicle position trajectories (from the entry point of the CZ at 450 m to the exit of MZ at 760 m, note that the entry of the MZ is at 750 m) for 200 s solved by the proposed methodology subject to a CAV penetration rate of 50% and a balanced traffic volume of 1000 veh/h across all lanes. The trajectories of HDVs are denoted by dashed lines, and the trajectories of CAVs are represented by solid lines. Only two perpendicular lanes, NS refers to the direction from north-to-south, and EW is the direction from east-to-west, are shown for clarity of the figure.

in the MZ at the same time) and all vehicles follow the traffic lights, which verifies the feasibility of the proposed approach.

Additionally, considering that all vehicles are conventional, the resulting intersection vehicle throughput and average vehicle fuel consumption of the proposed method are compared with the results of the baseline approaches. As shown in Table II, an increase of 7.92% in the traffic throughput of intersections compared to the F-SPAT, while the proposed method achieves a similar result to O-SPAT and CVSC. The results imply that the throughput mainly depends on the signal control. The comparative results also show a reduction

TABLE II
VEHICLE THROUGHPUT AND AVERAGE FUEL USAGE COMPARISON BETWEEN THE PROPOSED METHOD AND THE BENCHMARK METHODS FOR A 200 S SIMULATION TRIAL.

	Vehicle throughput [veh]	Average fuel usage [mL]
Proposed	218	64.596
F-SPAT	202	68.558
O-SPAT	218	72.663
CVSC	218	68.691

in average fuel consumption of 12.49%, 6.13% and 6.34% when comparing the proposed method with F-SPAT, O-SPAT and CVSC, respectively. It can be understood that the speed optimization of CAVs plays a more critical role than the SPAT optimization in terms of fuel economy. In contrast to CVSC in [25], where speed profiles are determined by empirical rules, the proposed optimization of the speed trajectory can lead to more energy efficiency results without sacrificing traffic efficiency.

To examine the influence of traffic volume (arrival rate), we further compare the proposed approach with the three baseline algorithms under various scenarios, considering both balanced and unbalanced arrival rates across all lanes. Without loss of generality, the CAV penetration rate is set to 60%. The two top figures in Fig. 5 present the control solutions for three methods with a balanced arrival rate in all directions. The three methods exhibit comparable performance when dealing with a low traffic volume case, 400 veh/h/lane. As traffic volume increases, the proposed method, CVSC [25] and O-SPAT can result in better throughput compared to F-SPAT, and the maximum benefit of 8.65% is achieved at 1170 veh/h/lane. In addition, the proposed method costs the least fuel due to joint control of the SPAT and the vehicle speed trajectory. As traffic volume increases, the proposed method shows an improved energy efficiency compared to O-SPAT, and the benefit is maximized at 12.65% when the arrival rate reaches 1170 veh/h/lane. Compared to CVSC, the proposed method can achieve a maximum improvement of 8.67% in fuel consumption. Although the fuel savings of the proposed method are not as high when compared to F-SPAT, it remains the best for all arrival rates.

The unbalanced cases are illustrated at the bottom of Fig. 5. The aggregated arrival rates of any two perpendicular approaches are fixed at 2000 veh/h whereas the arrival rates for any two opposite directions are identical. It is important to highlight that only F-SPAT and the CVSC are depicted for comparison, whereas O-SPAT can attain comparable throughput to the proposed method; however, its energy efficiency is significantly compromised, as observed in the top two plots in Fig. 5 and Table II. The proposed method results in a traffic throughput performance comparable to that of the CVSC method while showing a significant improvement compared to F-SPAT. The improvement of the proposed method in terms of throughput becomes more pronounced as the level of imbalance intensifies. In particular, in the scenario with a volume distribution of 400/1600 veh/h/lane, the benefit amounts to 14.10%, which is significantly higher than the 7.12% achieved in the case of 1000/1000 veh/h/lane. Regarding fuel consumption, a similar conclusion can be drawn based on the results compared to F-SPAT and CVSC, where maximum improvements of 8. 33% and 7.22% are observed, respectively, when the volume distribution follows 400/1600 veh/h/lane.

Fig. 6 presents a speed comparison between the proposed method and the other three benchmark algorithms. The balanced case is shown on the left, where the CAV penetration rate is set to 60%. The proposed algorithm can lead to a higher average speed compared to the other three methods in all cases.

In the balanced case, F-SPAT can outperform O-SPAT when the volume is low, but as the volume of traffic increases, the performance of F-SPAT degrades and becomes the least-performing method. The proposed method and CVSC [25] can outperform both F-SPAT and O-SPAT for all traffic volumes,

This article has been accepted for publication in IEEE Transactions on Transportation Electrification. This is the author's version which has not been fully edited and content may change prior to final publication. Citation information: DOI 10.1109/TTE.2024.3394595

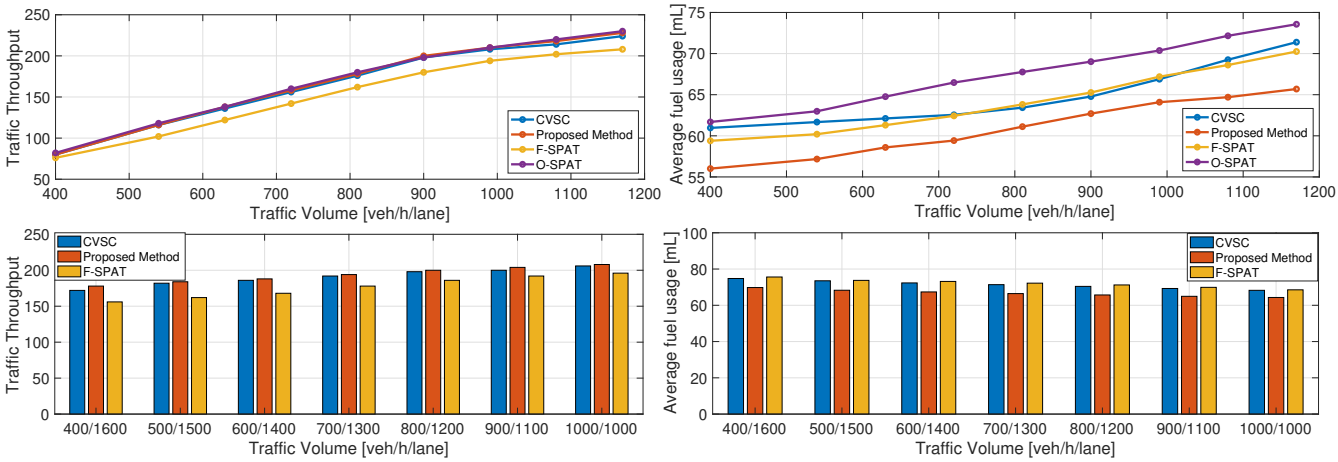

Fig. 5. Intersection traffic throughput and average fuel consumption of the proposed and benchmark methods under balanced and unbalanced traffic volume across the lanes subject to a CAV penetration rate of 60%. Top: balanced cases. Bottom: unbalanced across a pair of perpendicular lanes with an aggregated arrival rate of 2000 veh/h. The opposite directions have the same traffic volume.

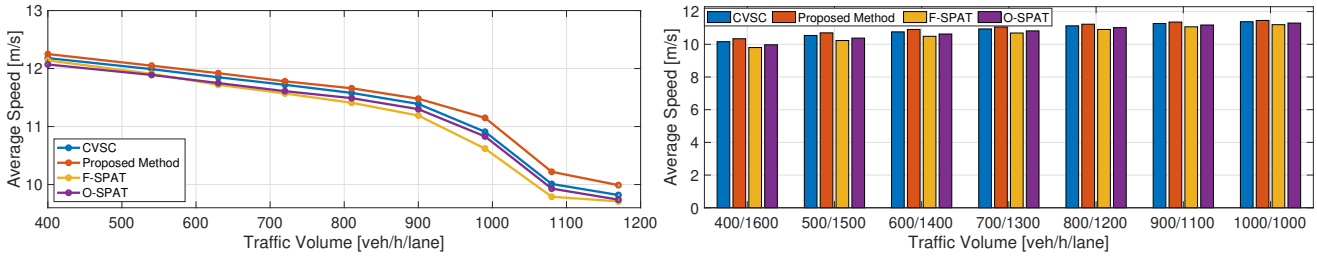

Fig. 6. Average speed of the proposed and benchmark methods under balanced and unbalanced traffic volume across the lanes subject to a CAV penetration rate of 60%. Left: balanced cases. Right: unbalanced across a pair of perpendicular lanes with an aggregated arrival rate of 2000 veh/h. The opposite directions have the same traffic volume.

while the fastest average speed is always achieved by the proposed method. More specifically, the proposed method shows an improved average speed compared to O-SPAT, which is maximized at 2.95% when the arrival rate reaches 1080 veh/h/lane. Compared to CVSC, the proposed method can achieve a maximum improvement of 2.20% in average speed.

The unbalanced case is illustrated on the right. The proposed method results in slightly faster average speed performance compared to the other three methods when the level of imbalance is low. The improvement of the proposed method in terms of average speed becomes more significant as the level of imbalance increases. In particular, in the scenario with a volume distribution of 400/1600 veh/h/lane, the benefit amounts to 6.55%, 4.71%, and 2.77% when compared with the F-SPAT, the O-SPAT, and the CVSC method, respectively.

To assess how the adoption of EVs impacts the energy efficiency of the proposed method, three different scenarios with 100%, 50%, and 0% EV penetration rates are examined. For illustrative purposes, we base our analysis on a scenario featuring an evenly distributed traffic volume of 1000 veh/h across all lanes, and a CAV penetration rate of 60%. We subsequently evaluate energy consumption using equations (36) to (38). It is noteworthy that in the 50% EV penetration scenario, all EVs are also CAVs, as automation often coincides with electrification. As illustrated in Fig.7, an increase in the penetration of EVs leads to a substantial reduction in energy consumption. This is because of the improved efficiency of electric drives and the occurrence of numerous stop-and-go situations at intersections.

Finally, the influence of the CAV penetration rate, ranging

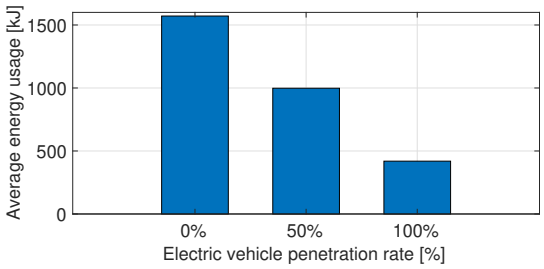

Fig. 7. The impact of EV penetration rate on the vehicle energy efficiency subject to a 1000 veh/h/lane traffic volume and a fixed 60% CAV penetration rate.

from 30% to 100%, on the energy consumption and vehicle throughput of the proposed method is investigated under a fully electric environment. In this specific case, it is assumed that the volume of vehicles is evenly distributed in all directions. As shown in the left plot of Fig. 8, the traffic throughput is primarily influenced by traffic volume rather than penetration rate. In principle, the throughput increases linearly as the volume rises, but it peaks at about 1200 veh/h/lane, which represents the capacity for the lane. As previously mentioned, the traffic throughput is heavily influenced by SPAT control, which greatly relies on the knowledge of the vehicle location. As uncertainties are not considered in the present work, the benefit of additional automation may not be readily apparent, particularly when the traffic volume is low. However, in high-traffic volume scenarios, an increased number of CAVs can have a more positive impact on SPAT

optimization, thereby improving traffic throughput. The impact of the penetration rate on traffic throughput becomes most evident when the traffic volume reaches 1000 veh/h/lane. With a penetration rate of 100%, traffic throughput can be improved by 5.03% compared to the 30% case. In contrast, the average electricity consumption, as presented in the right plot of Fig. 8, can be reduced when the CAV penetration rises, given the same traffic volume. This reduction becomes slightly more pronounced with higher traffic volumes. This can be understood as follows: 1) the energy cost is primarily influenced by optimizing speed trajectories, and as the penetration rate increases, more vehicles can be precisely controlled, allowing for faster platoon formation, and therefore greater energy savings; and 2) vehicle movement is less restrained by safety constraints in low traffic volume cases, thereby fewer acceleration and deceleration during driving are required. The most apparent energy reduction caused by an increase in the penetration rate occurs when the traffic volume is 1200 veh/h/lane, with a reduction of 11.47%.

V. CONCLUSIONS

This paper introduces a two-layer intersection signal-vehicle coupled coordination scheme for joint control of intersection traffic signal phase and time (SPAT) and speed trajectory of connected and autonomous vehicles (CAV) and human-driven vehicles (HDV). The method is developed based on a CAV-led mixed platoon model, where the motion of the HDVs is governed by a linearized intelligent driver model. In addition to the SPAT, the target platoon velocity and the number of passing platoons are continuously updated in the upper layer to minimize the total waiting time. Subsequently, the intersection controller utilizes the SPAT information to conduct optimal control of the mixed platoon within the control zone by manipulating the speed of the leading CAVs.

A comparative analysis is performed, contrasting the proposed method with conventional approaches focusing solely on optimizing signal duration or vehicle trajectory, as well as a recently proposed coupled vehicle-signal control method [25]. Through these comparisons, the advantages of the proposed method are revealed in terms of average fuel consumption and traffic throughput. The proposed method improves throughput by 7.92% while achieving additional fuel savings of 5.97% compared to the method with optimized vehicle trajectories only. Furthermore, it reduces fuel consumption by 11.54% compared to the benchmark method, which solely optimizes SPTA, and shows a reduction of 6.34% compared to a state-of-the-art method [25] while maintaining a similar traffic throughput. The simulation results also highlight the significant roles of SPAT control and vehicle trajectory control in enhancing throughput and achieving energy savings, respectively. The benefits of the proposed control solution are further amplified in the presence of unbalanced traffic volumes across the intersection lanes. Lastly, the simulation results validate the advantages of increasing the CAV market penetration rate, particularly in terms of electricity savings, which can reach as high as 11.47% when the penetration is escalated from 30% to 100% in the given simulation.

In future research, cooperative control of SPAT and speed trajectory at the network level will be further investigated. Using analytical modeling to solve the network-level SPAT optimization is challenging due to the high dimension of the problem. Thus, we may rely on some learning-based method to conduct SPAT optimization and vehicle routing at the network level and try to find effective and trustworthy optimized control strategies in real-world applications.

REFERENCES

[1] J. Rios-Torres and A. A. Malikopoulos, "A survey on the coordination of connected and automated vehicles at intersections and merging at highway on-ramps," *IEEE Transactions on Intelligent Transportation Systems*, vol. 18, no. 5, pp. 1066–1077, 2017.

[2] J. Guanetti, Y. Kim, and F. Borrelli, "Control of connected and automated vehicles: State of the art and future challenges," *Annual reviews in control*, vol. 45, pp. 18–40, 2018.

[3] X. Pan, B. Chen, S. Timotheou, and S. A. Evangelou, "A convex optimal control framework for autonomous vehicle intersection crossing," *IEEE Transactions on Intelligent Transportation Systems*, vol. 24, no. 1, pp. 163–177, 2023.

[4] Z. Zhong, M. Nejad, and E. E. Lee, "Autonomous and semiautonomous intersection management: A survey," *IEEE Intelligent Transportation Systems Magazine*, vol. 13, no. 2, pp. 53–70, 2021.

[5] H. Yang, H. Rakha, and M. V. Ala, "Eco-cooperative adaptive cruise control at signalized intersections considering queue effects," *IEEE Transactions on Intelligent Transportation Systems*, vol. 18, no. 6, pp. 1575–1585, 2017.

[6] T. Tan, F. Bao, Y. Deng, A. Jin, Q. Dai, and J. Wang, "Cooperative deep reinforcement learning for large-scale traffic grid signal control," *IEEE Transactions on cybernetics*, vol. 50, no. 6, pp. 2687–2700, 2020.

[7] X. Tang, G. Zhong, S. Li, K. Yang, K. Shu, D. Cao, and X. Lin, "Uncertainty-aware decision-making for autonomous driving at uncontrolled intersections," *IEEE Transactions on Intelligent Transportation Systems*, vol. 24, no. 9, pp. 9725–9735, 2023.

[8] X. Pan, B. Chen, L. Dai, S. Timotheou, and S. A. Evangelou, "A hierarchical robust control strategy for decentralized signal-free intersection management," *IEEE Transactions on Control Systems Technology*, vol. 31, no. 5, pp. 2011–2026, 2023.

[9] J. Li, C. Yu, Z. Shen, Z. Su, and W. Ma, "A survey on urban traffic control under mixed traffic environment with connected automated vehicles," *Transportation Research Part C: Emerging Technologies*, vol. 154, p. 104258, 2023.

[10] K. Yang, X. Tang, S. Qiu, S. Jin, Z. Wei, and H. Wang, "Towards robust decision-making for autonomous driving on highway," *IEEE Transactions on Vehicular Technology*, vol. 72, no. 9, pp. 11 251–11 263, 2023.

[11] Y. Feng, L. Head, S. Khoshmagham, and M. Zamanipour, "A real-time adaptive signal control in a connected vehicle environment," *Transportation Research Part C: Emerging Technologies*, vol. 55, pp. 460–473, 2015.

[12] W. Liu, G. Qin, H. Yun, and J. Fei, "Distributed cooperative reinforcement learning-based traffic signal control that integrates v2x networks' dynamic clustering," *IEEE Transactions on Vehicular Technology*, vol. 66, no. 10, pp. 8667–8681, 2017.

[13] T. Chu, J. Wang, L. Codeca, and Z. Li, "Multi-agent deep reinforcement learning for large-scale traffic signal control," *IEEE Transactions on Intelligent Transportation Systems*, vol. 21, no. 3, pp. 1086–1095, 2020.

[14] W. Zhao, D. Ngoduy, S. Shepherd, R. Liu, and M. Papageorgiou, "A platoon based cooperative eco-driving model for mixed automated and human-driven vehicles at a signalised intersection," *Transportation Research Part C: Emerging Technologies*, vol. 95, pp. 802–821, 2018.

[15] X. Li, A. Ghiasi, and Z. Xu, "A piecewise trajectory optimization model for connected automated vehicles: Exact optimization algorithm and queue propagation analysis," *Transportation Research Part B: Methodological*, vol. 118, pp. 429–456, 11 2018.

[16] Y. Guo, J. Ma, C. Xiong, X. Li, F. Zhou, and W. Hao, "Joint optimization of vehicle trajectories and intersection controllers with connected automated vehicles: Combined dynamic programming and shooting heuristic approach," *Transportation Research Part C: Emerging Technologies*, vol. 98, pp. 54–72, 01 2019.

[17] Y. Feng, C. Yu, and H. Liu, "Spatiotemporal intersection control in a connected and automated vehicle environment," *Transportation Research Part C: Emerging Technologies*, vol. 89, pp. 364 – 383, 2018.

[18] B. Xu, X. J. Ban, Y. Bian, W. Li, J. Wang, S. E. Li, and K. Li, "Cooperative method of traffic signal optimization and speed control of connected vehicles at isolated intersections," *IEEE Transactions on Intelligent Transportation Systems*, vol. 20, no. 4, pp. 1390–1403, 2019.

[19] Z. Li, L. Elefteriadou, and S. Ranka, "Signal control optimization for automated vehicles at isolated signalized intersections," *Transportation Research Part C: Emerging Technologies*, vol. 49, pp. 1–18, 2014.

[20] C. Yu, Y. Feng, H. X. Liu, W. Ma, and X. Yang, "Integrated optimization of traffic signals and vehicle trajectories at isolated urban intersections," *Transportation Research Part B: Methodological*, vol. 112, no. JUN., pp. 89–112, 2018.

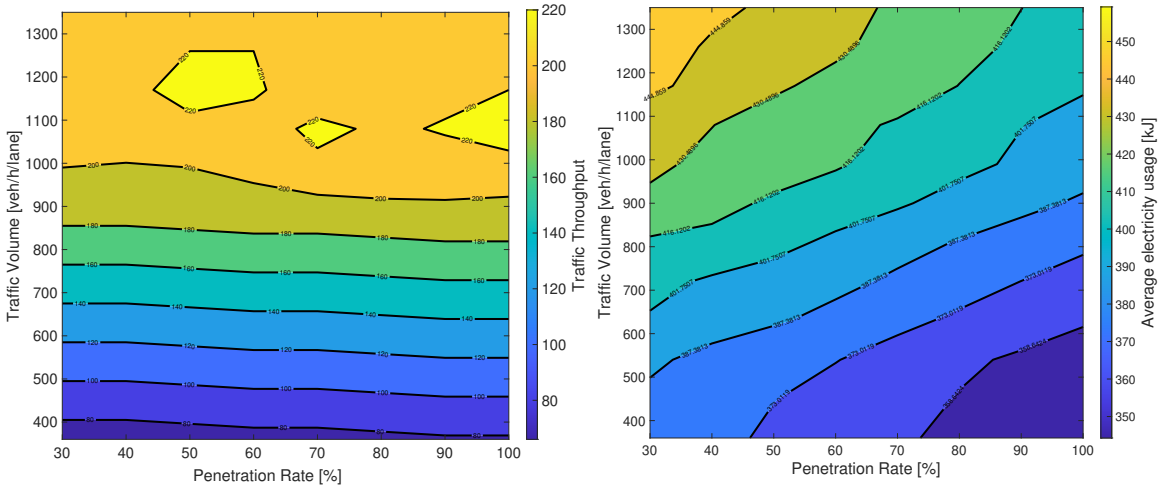

Fig. 8. Intersection traffic throughput and average electricity consumption of the proposed method obtained under different CAV penetration rates and traffic volumes.

[21] M. Liu, J. Zhao, S. Hoogendoorn, and M. Wang, "A single-layer approach for joint optimization of traffic signals and cooperative vehicle trajectories at isolated intersections," *Transportation Research Part C: Emerging Technologies*, vol. 134, no. 103459, 2022.

[22] X. Jiang and Q. Shang, "A dynamic CAV-dedicated lane allocation method with the joint optimization of signal timing parameters and smooth trajectory in a mixed traffic environment," *IEEE Transactions on Intelligent Transportation Systems*, vol. 24, no. 6, pp. 6436–6449, 2023.

[23] X. Huang, P. Lin, M. Pei, B. Ran, and M.-C. Tan, "Reservation-based cooperative ecodriving model for mixed autonomous and manual vehicles at intersections," *IEEE Transactions on Intelligent Transportation Systems*, vol. 24, no. 9, pp. 9501–9517, 2023.

[24] M. Tajali and A. Hajbabaie, "Traffic signal timing and trajectory optimization in a mixed autonomy traffic stream," *IEEE Transactions on Intelligent Transportation Systems*, vol. 23, no. 7, pp. 6525–6538, 2022.

[25] Y. Du, W. Shangguan, and L. Chai, "A coupled vehicle-signal control method at signalized intersections in mixed traffic environment," *IEEE Transactions on Vehicular Technology*, vol. 70, no. 3, pp. 2089–2100, 2021.

[26] P. Sun, D. Nam, R. Jayakrishnan, and W. Jin, "An eco-driving algorithm based on vehicle to infrastructure (v2i) communications for signalized intersections," *Transportation Research Part C: Emerging Technologies*, vol. 144, p. 103876, 2022.

[27] X. J. Liang, S. I. Guler, and V. V. Gayah, "Joint optimization of signal phasing and timing and vehicle speed guidance in a connected and autonomous vehicle environment," *Transportation Research Record*, vol. 2673, no. 4, pp. 70–83, 2019.

[28] R. Niroumand, M. Tajali, L. Hajibabai, and A. Hajbabaie, "Joint optimization of vehicle-group trajectory and signal timing: Introducing the white phase for mixed-autonomy traffic stream," *Transportation Research Part C: Emerging Technologies*, vol. 116, p. 102659, 2020.

[29] R. Niroumand, L. Hajibabai, A. Hajbabaie, and M. Tajali, "Effects of autonomous driving behavior on intersection performance and safety in the presence of white phase for mixed-autonomy traffic stream," *Transportation Research Record: Journal of the Transportation Research Board*, vol. 2676, no. 8, pp. 112–130, 2022.

[30] M. Pourmehrab, L. Elefteriadou, S. Ranka, and M. Martin-Gasulla, "Optimizing signalized intersections performance under conventional and automated vehicles traffic," *IEEE Transactions on Intelligent Transportation Systems*, vol. 21, no. 7, pp. 2864–2873, 2020.

[31] Z. Yao, Z. Bin, Y. Tengfei, H. Jiang, and Y. Jiang, "Reducing gasoline consumption in mixed connected automated vehicles environment: A joint optimization framework for traffic signals and vehicle trajectory," *Journal of Cleaner Production*, vol. 265, p. 121836, 2020.

[32] Yang, Kaidi, Guler, S., Ilgin, Menendez, and Monica, "Isolated intersection control for various levels of vehicle technology: Conventional, connected, and automated vehicles," *Transportation research, Part C: Emerging technologies*, vol. 72, pp. 109–129, 2016.

[33] H. Liu, X. Lu, and S. Shladover, "Traffic signal control by leveraging cooperative adaptive cruise control (CACC) vehicle platooning capabilities," *Transportation Research Part C: Emerging Technologies*, vol. 104, pp. 390–407, 2019.

[34] B. Li, W. Zhuang, H. Zhang, H. Sun, H. Liu, J. Zhang, G. Yin, and B. Chen, "Traffic-aware ecological cruising control for connected electric vehicle," *IEEE Transactions on Transportation Electrification*, pp. 1–1, 2023.

[35] B. Li, W. Zhuang, H. Zhang, R. Zhao, H. Liu, L. Qu, J. Zhang, and B. Chen, "A comparative study of energy-oriented driving strategy for connected electric vehicles on freeways with varying slopes," *Energy*, vol. 289, p. 129916, 2023.

[36] T. Ghoul and T. Sayed, "Real-time signal-vehicle coupled control: An application of connected vehicle data to improve intersection safety," *Accident; Analysis and Prevention*, vol. 162, p. 106389, 2021.

[37] Y. Guo and J. Ma, "DRL-TP3: A learning and control framework for signalized intersections with mixed connected automated traffic," *Transportation Research Part C: Emerging Technologies*, vol. 132, p. 103416, 2021.

[38] M. Tang, W. Zhuang, B. Li, H. Liu, Z. Song, and G. Yin, "Energy-optimal routing for electric vehicles using deep reinforcement learning with transformer," *Applied Energy*, vol. 350, p. 121711, 2023.

[39] J. Wang, Y. Zheng, C. Chen, Q. Xu, and K. Li, "Leading cruise control in mixed traffic flow: System modeling, controllability, and string stability," *IEEE Transactions on Intelligent Transportation Systems*, vol. 23, pp. 12 861 – 12 876, 2022.

[40] C. Chen, J. Wang, Q. Xu, J. Wang, and K. Li, "Mixed platoon control of automated and human-driven vehicles at a signalized intersection: Dynamical analysis and optimal control," *Transportation Research Part C: Emerging Technologies*, vol. 127, p. 103138, 2021.

[41] S. Chen and D. J. Sun, "An improved adaptive signal control method for isolated signalized intersection based on dynamic programming," *IEEE Intelligent Transportation Systems Magazine*, vol. 8, no. 4, pp. 4–14, 2016.

[42] W. Li and X. Ban, "Connected vehicles based traffic signal timing optimization," *IEEE Transactions on Intelligent Transportation Systems*, vol. 20, no. 12, pp. 4354–4366, 2019.

[43] C. Chen, M. Cai, J. Wang, K. Li, Q. Xu, J. Wang, and K. Li, "Cooperation method of connected and automated vehicles at unsignalized intersections: Lane changing and arrival scheduling," *IEEE Transactions on Vehicular Technology*, vol. 71, no. 11, pp. 11 351–11 366, 2022.

[44] M. Treiber, A. Hennecke, and D. Helbing, "Congested traffic states in empirical observations and microscopic simulations," *Physical Review E*, vol. 62, pp. 1805–1824, 2000.

[45] J. Hu, P. Bhowmick, F. Arvin, A. Lanzon, and B. Lennox, "Cooperative control of heterogeneous connected vehicle platoons: An adaptive leader-following approach," *IEEE Robotics and Automation Letters*, vol. 5, no. 2, pp. 977–984, 2020.

[46] K. de Winkel, T. Irmak, R. Happee, and B. Shyrokau, "Standards for passenger comfort in automated vehicles: Acceleration and jerk," *Applied Ergonomics*, vol. 106, p. 103881, 2023.

[47] M. Kamal, M. Mukai, J. Murata, and T. Kawabe, "Ecological vehicle control on roads with up-down slopes," *IEEE Transactions on Intelligent Transportation Systems*, vol. 12, no. 3, pp. 783–794, 2011.